Effects of hydrogen trapping particles on environmentally assisted fatigue fracture of Al-Zn-Mg alloy

Toda, Hiroyuki
Department of Mechanical Engineering, Kyushu University

Fujihara, Hiro
Department of Mechanical Engineering, Kyushu University

Inamori, Akito
Department of Mechanical Engineering, Kyushu University

Shimizu, Kazuyuki
Department of Mechanical and Physical Engineering, Tottori University

他

出版情報：International Journal of Fatigue. 209, pp.109622-, 2026-08. Elsevier
バージョン：

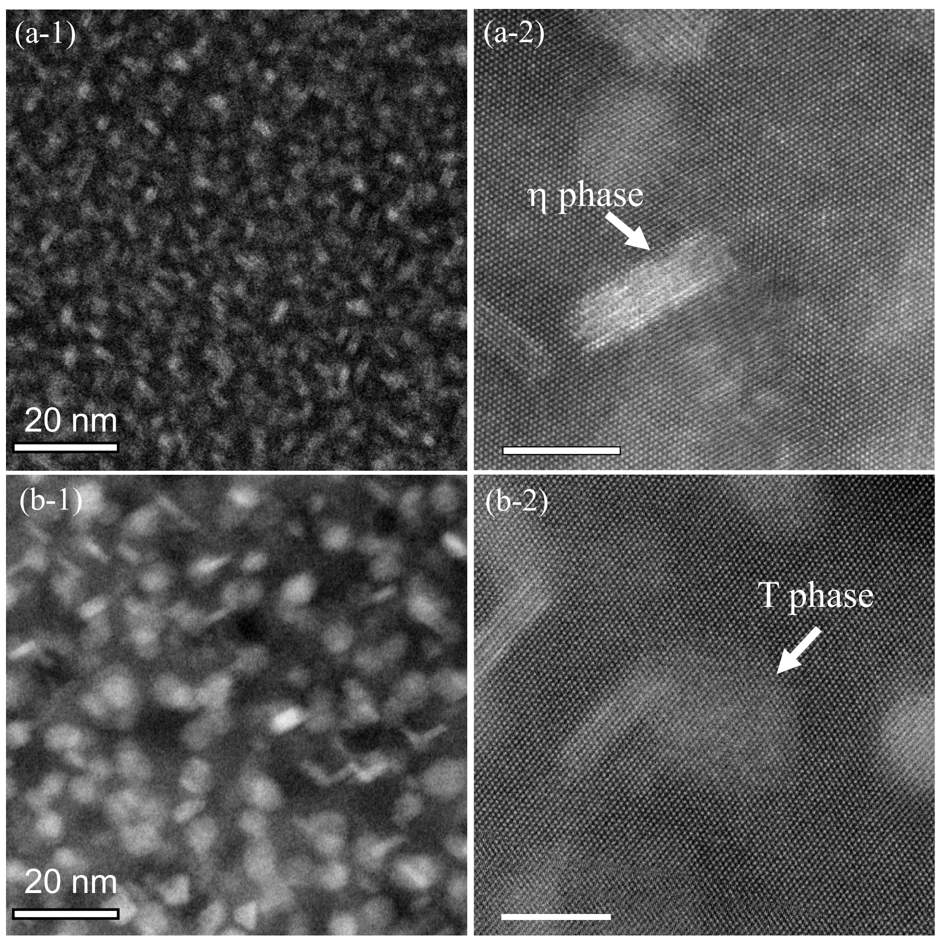

Fig. 1 Bright field TEM micrographs of (a-1) material η and (b-1) materials T. (a-2) and (b-2) are the ultra-high resolution lattice images of the two materials.

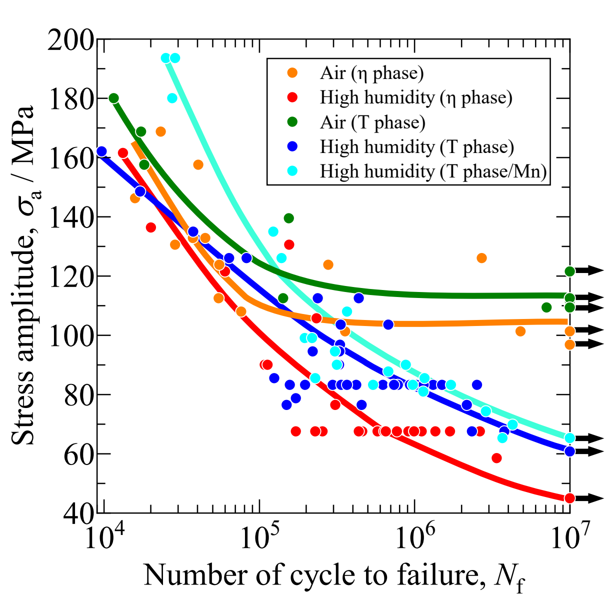

Fig. 2 S-N curves for the three materials tested under the high humidity and atmospheric environments.

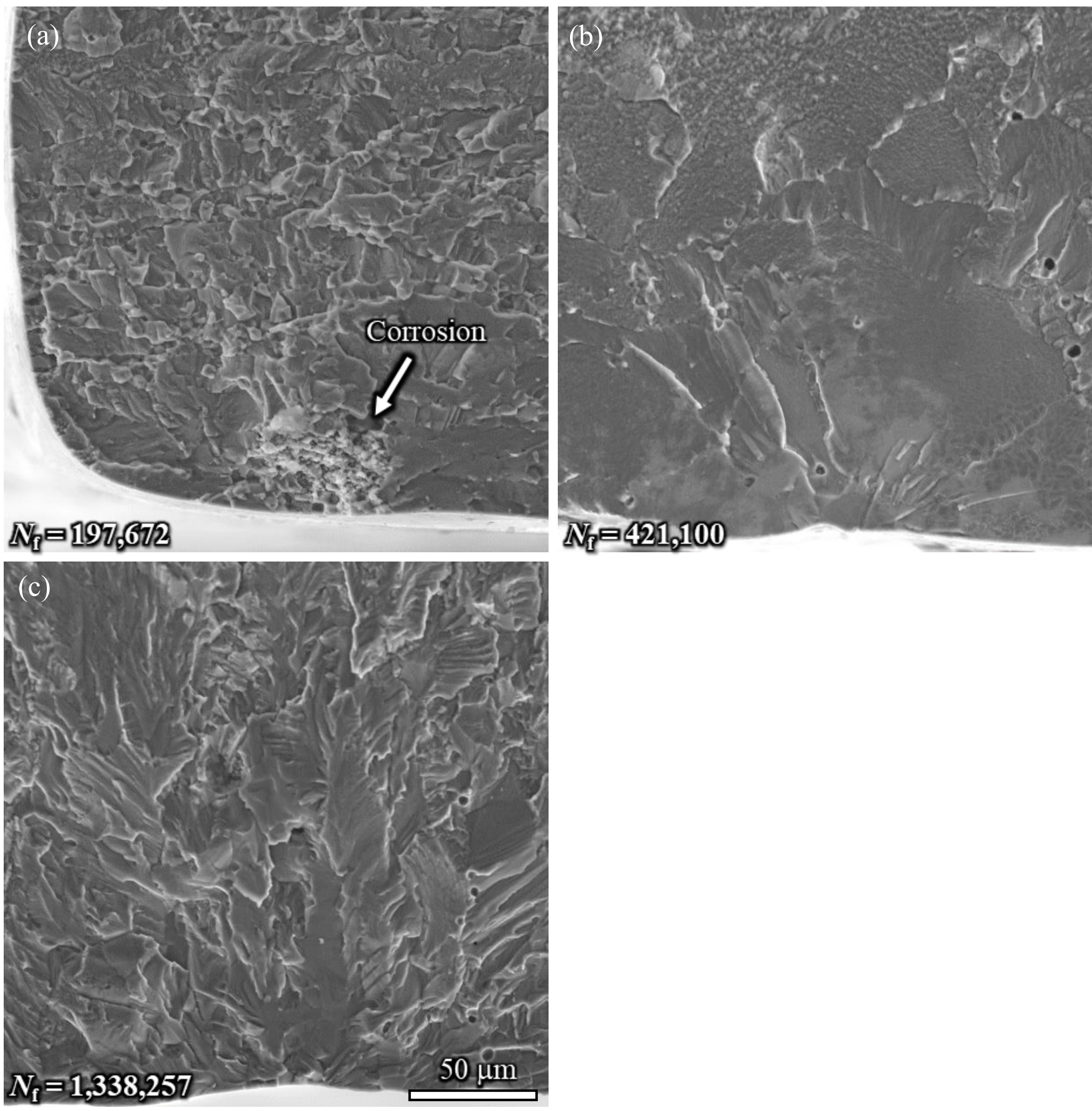

Fig. 3 SEM observations of representative fracture surfaces after fatigue testing. (a) / (b) and (c) show fracture surfaces for fatigue lifetimes of 10^5 and 10^6 cycle orders, respectively. (a) shows a fatigue crack originating from a corrosion product in the fatigue test of material T under the high humidity environment. (b) and (c) show fatigue cracks directly originating from the surface, rather than originating from corrosion product, in material η under the high humidity environment and material T under the atmospheric environment, respectively.

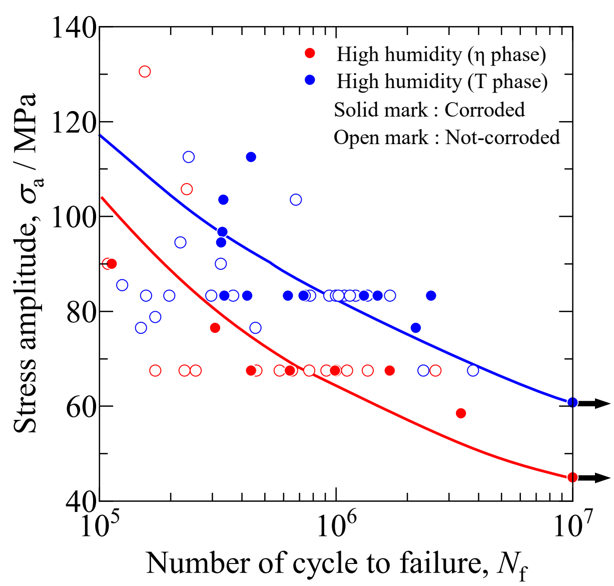

Fig. 4 Revised S-N curves of materials η and T in which the data points from the high humidity environment depicted in Fig. 2 have been distinguished by the presence or absence of corrosion products in proximity to the crack initiation points on the fracture surface.

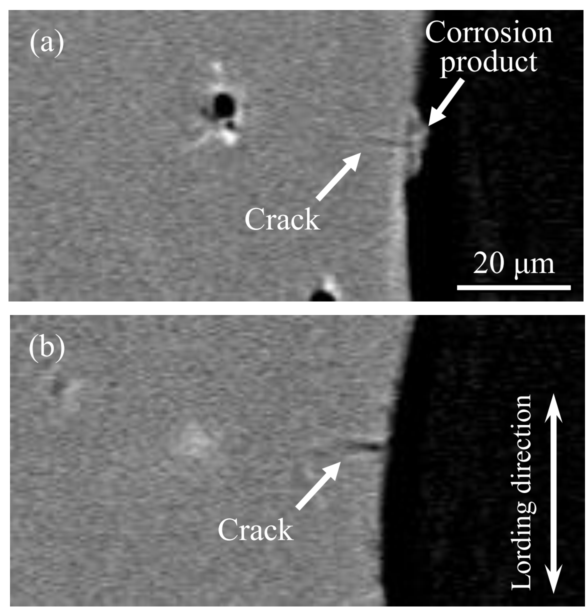

Fig. 5 Virtual cross-sections of 3D images, representing two distinct types of fatigue crack in material η observed under the high humidity environment. The first type (a) originates from corrosion product, while the second type (b) originates directly from the surface of the material without originating from corrosion product.

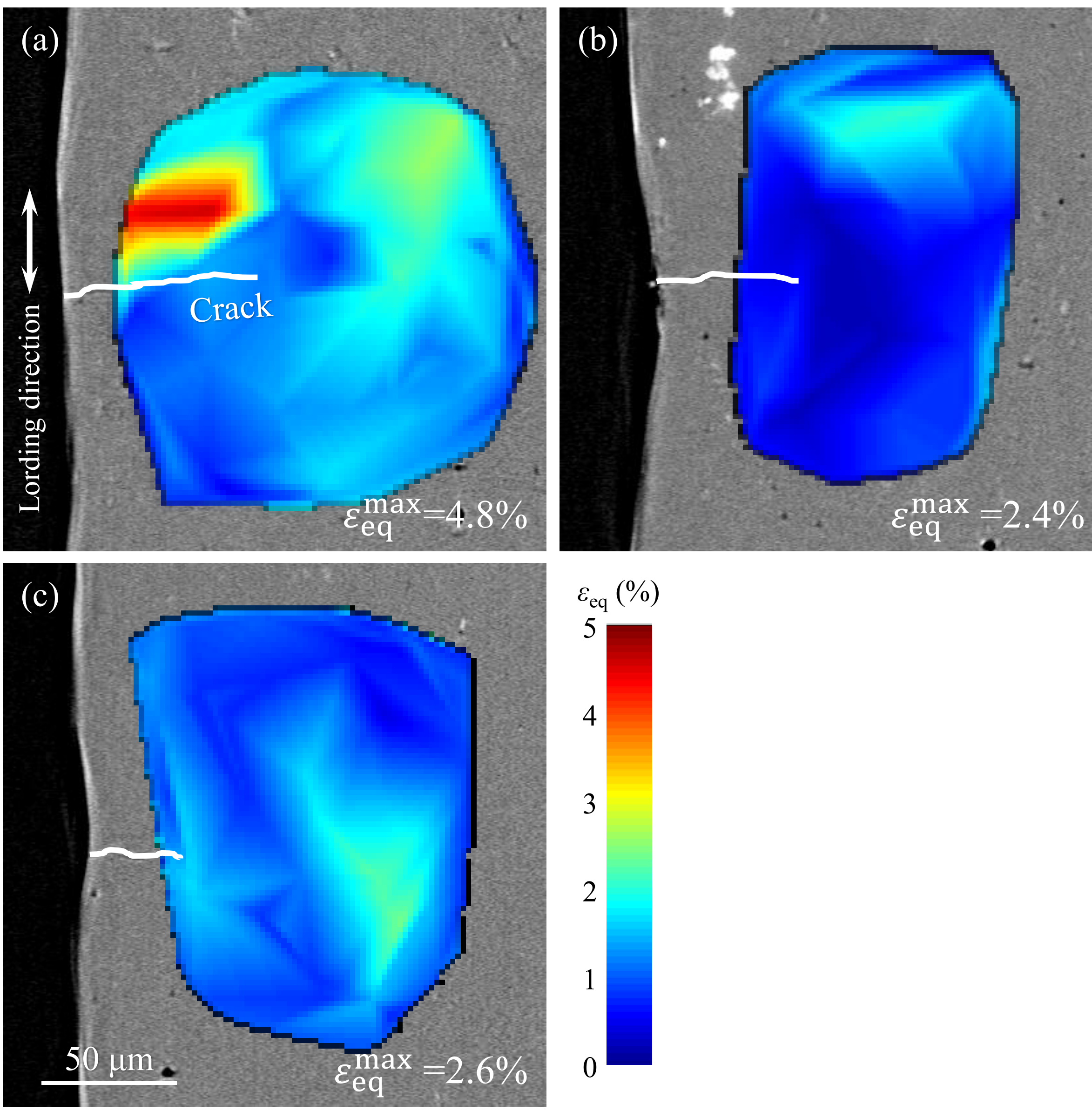

Fig. 6 The results of the 3D plastic strain mapping near the fatigue crack tips for (a) material η, and (b) and (c) material T. (a)/(b) and (c) are the high humidity and atmospheric environments, respectively. The maximum equivalent strain value measured in the region of interest is shown in each figure.

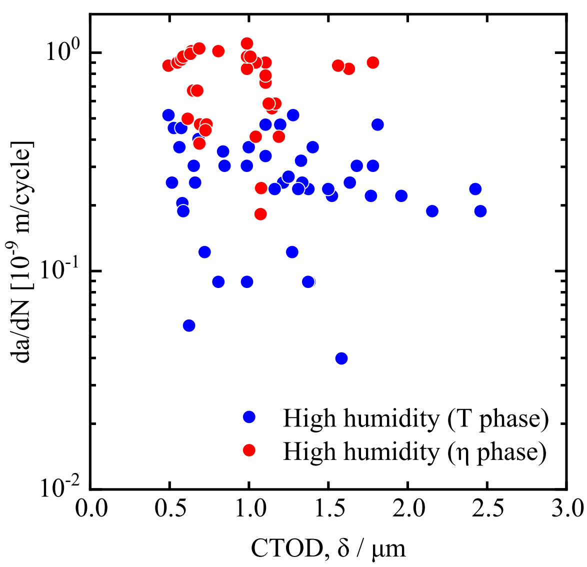

Fig. 7 Relationship between CTOD and crack propagation rate for materials η and T tested in the high humidity environment.

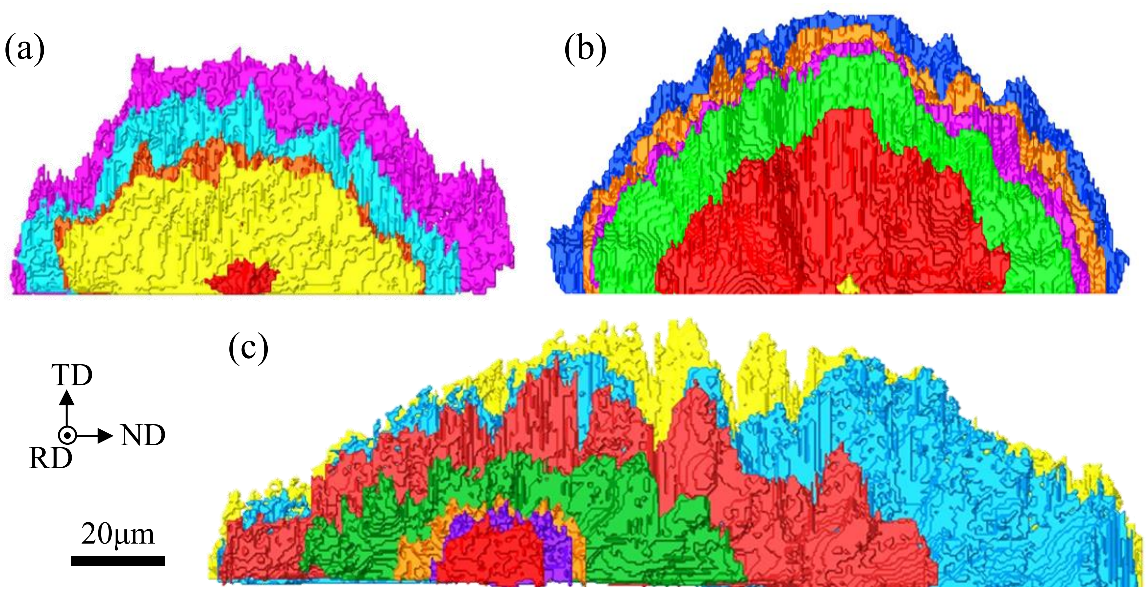

Fig. 8 Changes in fatigue crack morphology accompanying crack propagation. The differently coloured crack images are top-down views (RD direction) of 3D crack images captured at different loading cycles. (a) material η in the high humidity environment, (b) material T in the atmospheric environment, and (c) material T in the high humidity environment. The number of cycles captured: (a) 950,000 (red), 1,197,000 (yellow), 1,200,200 (orange), 1,214,200 (light blue), and 1,217,200 (violet) cycles. (b) 1,930,000 (yellow), 2,330,000 (red), 2,335,000 (green), 2,335,800 (violet), 2,337,300 (orange), and 2,338,500 (blue) cycles. (c) 1,145,000 (red), 1,175,000 (blue), 1,205,000 (orange), 1,235,000 (green), 1,265,000 (red), 1,295,000 (light blue), and 1,325,000 (yellow) cycles.

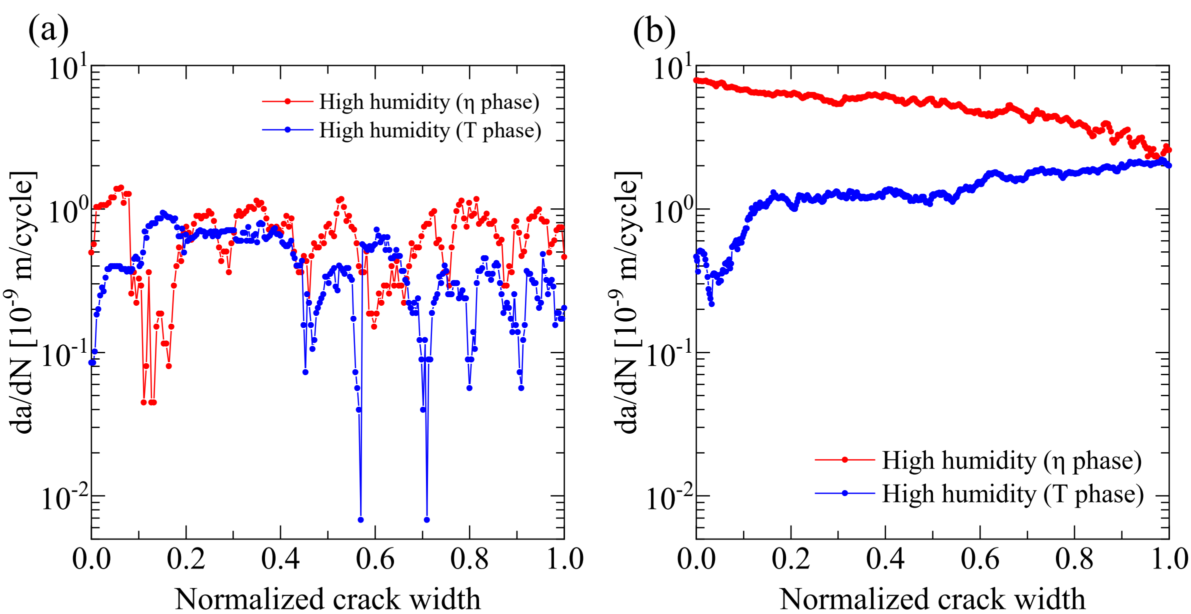

Fig. 9 The variations in crack propagation rate along the crack front lines. (a) the data for the high humidity environment of materials η and T at crack lengths of 45 μm and 47 μm, respectively, and (b) the data for the high humidity environment of materials η and T at crack lengths of 136 μm and 156 μm, respectively.

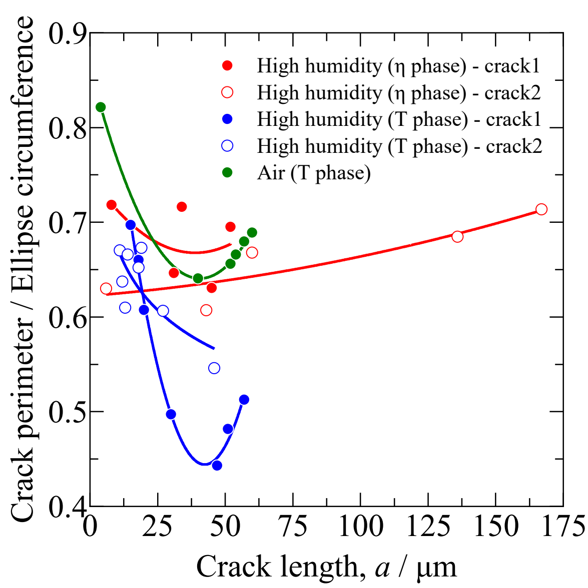

Fig. 10 The variations in the crack front shape shown in Fig. 8, which have been approximated as ellipses, and the ratio of ellipse's semi-circumference to crack front line length is expressed as a quantitative indicator of complex crack front shape.

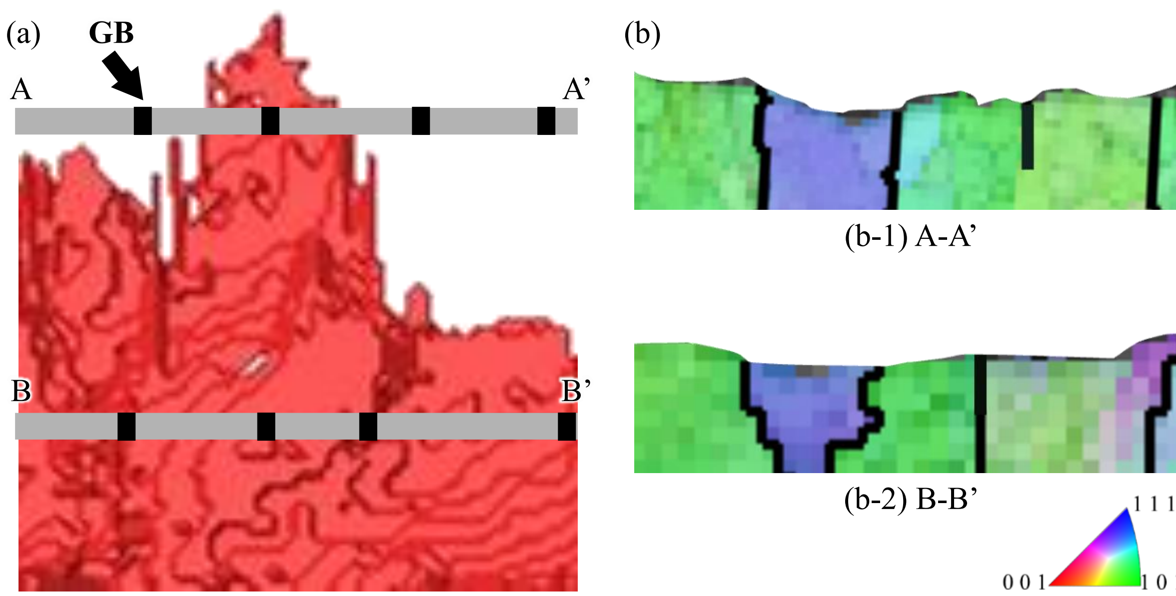

Fig. 11 The fracture surface of material T in the high humidity environment was partly ground away to a specified depth from the surface. Polycrystalline microstructures were obtained by the EBSD analysis at two cross-sections indicated by A-A' and B-B' in the figure, and compared with the crack front shape. Positions where the crack propagation velocity decreased or increased relative to the average correspond to high-angle grain boundaries with an orientation difference of 15^{o} or more.

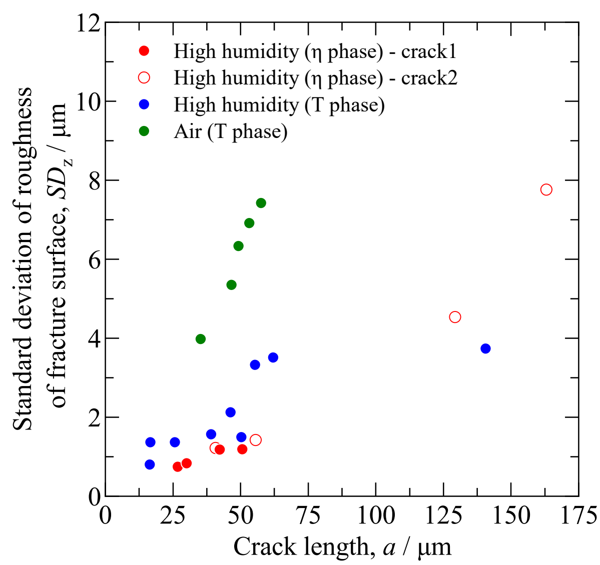

Fig. 12 Standard deviation values of crack surface coordinates, presented as a measure of fatigue crack deflection or tilting caused by crack propagation driving forces in modes II and III.